Journal of Membrane Science 593 (2020) 117440

Contents lists available at ScienceDirect

Journal of Membrane Science

journal homepage: www.elsevier.com/locate/memsci

Relationship between ethane and ethylene diffusion inside ZIF-11 crystals confined in polymers to form mixed-matrix membranes

Evan M. Forman[a], Amineh Baniani[a], Lei Fan[a], Kirk J. Ziegler[a], Erkang Zhou[b], Fengyi Zhang[b], Ryan P. Lively[b], Sergey Vasenkov[a,*]

[a] Department of Chemical Engineering, University of Florida, Gainesville, FL, 32611, USA
[b] School of Chemical & Biomolecular Engineering, Georgia Institute of Technology, Atlanta, GA, 30332, USA

ARTICLE INFO

Keywords:
Diffusion
PFG NMR
Gas separations
Mixed-matrix membranes
ZIF-11

ABSTRACT

Self-diffusivities of ethane were measured by multinuclear pulsed field gradient (PFG) NMR inside zeolitic imidazolate framework-11 (ZIF-11) crystals dispersed in several selected polymers to form mixed-matrix membranes (MMMs). These diffusivities were compared with the corresponding intracrystalline self-diffusivities in ZIF-11 crystal beds. It was observed that the confinement of ZIF-11 crystals in ZIF-11/Torlon MMM can lead to a decrease in the ethane intracrystalline self-diffusivity. Such diffusivity decrease was observed at different temperatures used in this work. PFG NMR measurements of the temperature dependence of the intracrystalline self-diffusivity of ethylene in the same ZIF-11/Torlon MMM revealed similar diffusivity decrease as well as an increase in the diffusion activation energy in comparison to those in unconfined ZIF-11 crystals in a crystal bed. These observations for ethane and ethylene were attributed to the reduction of the flexibility of the ZIF-11 framework due to the confinement in Torlon leading to a smaller effective aperture size of ZIF-11 crystals. Surprisingly, the intra-ZIF diffusion selectivity for ethane and ethylene was not changed appreciably by the confinement of ZIF-11 crystals in Torlon in comparison to the selectivity in a bed of ZIF-11 crystals. No ZIF-11 confinement effects leading to a reduction in the intracrystalline self-diffusivity of ethane and ethylene were observed for the other two studied MMM systems: ZIF-11/Matrimid and ZIF-11/6FDA-DAM. The absence of the confinement effect in the latter MMMs can be related to the lower values of the polymer bulk modulus in these MMMs in comparison to that in ZIF-11/Torlon MMM. In addition, there may be a contribution from possible differences in the ZIF-11/polymer adhesion in different MMM types.

1. Introduction

Mixed-matrix membranes (MMMs), membranes prepared by dispersing porous filler particles in a polymer matrix, have gained much attention for important gas separations over recent years. MMMs were introduced to enhance separation performance over polymeric membranes, which are notoriously limited in separations of gas mixtures by a trade-off between selectivity and permeability. MMMs benefit from straightforward fabrication procedures in combination with robust mechanical properties expected for polymeric films as well as superior separation properties of filler particles [1–12]. Lately, MMMs have seen an influx of progress in their fabrication methods, focusing on using metal-organic frameworks (MOFs) as filler particles. MOFs exhibit great tunability of their aperture size while their organic linkers result in a better affinity with the polymers compared to inorganic microporous fillers, such as zeolites, making MOFs good candidates as filler particles [1-3,6,7,9-12]. One particular class of MOFs, zeolitic imidazolate frameworks (ZIFs) has seen recent interest and has been implemented as fillers [3,5,9,11,13,14]. Their excellent chemical and thermal stability in addition to their good adhesion at polymer interfaces have made the ZIF family more promising fillers compared with many other MOF types [3,5,8,12].

There is a number of recent studies of ZIF-based MMMs reporting improved separation performance when comparing the MMM to their base polymer film [3-5,11-18]. In particular, ZIF-11, which consists of benzimidazole ligands and Zn^{2+} nodes arranged in a RHO topology (Fig. S1) [19–21], has been explored as a filler material for MMMs in both experimental [14,17] and simulations studies [4]. ZIF-11 has attracted attention due to its small crystallographic pore aperture size of 3.0 Å and cage size of 14.6 Å, which represent promising pore structure for molecular sieving of light gases [19,21,22]. Our recent short paper reports the ^{13}C pulsed field gradient (PFG) NMR measurements of one

* Corresponding author.
E-mail address: svasenkov@che.ufl.edu (S. Vasenkov).

https://doi.org/10.1016/j.memsci.2019.117440
Received 1 July 2019; Received in revised form 30 August 2019; Accepted 2 September 2019
Available online 03 September 2019

sorbate (ethylene) at a single temperature in ZIF-11 crystal beds and three ZIF-11-based MMMs at different ethylene loadings to perform an initial characterization of the transport properties of ZIF-11 as unconfined crystals and as crystals embedded in polymer matrices [23]. These microscopic measurements revealed a reduction in the intra-ZIF diffusivity of ethylene in one specific ZIF-11-based MMM, ZIF-11/Torlon MMM, in comparison to that in a bed of ZIF-11 crystals. At the same time, the other two studied ZIF-11 based MMMs prepared with Matrimid and 6FDA-DAM showed no effect of ZIF-11 confinement in polymers on intra-ZIF diffusivity. A tentative explanation of these results has been that confinement of ZIF-11 particles in the Torlon polymer leads to a reduced flexibility of the ZIF framework. Furthermore, the higher bulk modulus of Torlon (4.5 GPa [24,25]) compared to the other studied polymers, Matrimid (3.5 GPa [26]), and 6FDA-DAM (1.2 GPa [27]) could be the reason for a stronger confinement effect in ZIF-11/Torlon MMM.

A few years before the publication of the discussed above short paper on diffusion of ethylene in ZIF-11-based MMMs, Caro's group and our groups provided experimental evidence that confinement of other types of ZIF crystals in polymers can reduce framework flexibility of these crystals [13,28,29]. Similar effect of the suppression of gate opening in MOFs by introducing a polymer coating on top of MOF membranes was also observed later [30,31]. Most recently, Caro's group reported the possibility to transform ZIF-8 into polymorphs with rigid lattices by using an external electric field [32]. All these studies point at the potential for MOF framework flexibility reduction that can lead to a better performance of MOFs in membrane-based separations than would otherwise be predicted based on data reported for the neat MOF crystals.

This paper reports a detailed PFG NMR study of intracrystalline self-diffusion of ethane and ethylene at different temperatures and gas loadings in ZIF-11 crystals located inside mixed-matrix membranes prepared with the Torlon, Matrimid, and 6FDA-DAM polymers. A comparison between the intracrystalline self-diffusivities measured in the MMMs and loosely packed beds of ZIF-11 crystals is also presented and discussed. Diffusion measurements were performed using ^{1}H and ^{13}C PFG NMR utilizing a high field (17.6 T or 14 T) and high magnetic field gradients (up to 25 T/m) to obtain diffusivities for the length scales of displacements smaller than the mean size of the ZIF-11 crystals. The reported data provide information on the relative influence of the confinement of ZIF-11 crystals in the polymers on the intra-ZIF diffusivity of each studied gas for a broad range of the measurement conditions. For ZIF-11/Torlon MMM demonstrating the intra-ZIF diffusivity reduction in comparison to unconfined ZIF-11 crystals, activation energies of ethane and ethylene diffusion were calculated and analyzed in the context of the ZIF-11 framework flexibility. The results reported in this work demonstrate complexity of the microscale diffusion in ZIF-based MMMs that needs to be taken into account when designing such MMMs for particular separations.

2. Experimental

2.1. Preparation of ZIF-11

ZIF-11 crystals were synthesized via solvothermal method [21]. Benzimidazole (Alfa Aesar) was dissolved by methanol (VWR International) and 18% ammonium hydroxide solution with a mass ratio of 0.6:16.75:3.75. $Zn(O_2CCH_3)_2{\cdot}2H_2O$ (Alfa Aesar) was dissolved by methanol and toluene (VWR International) with a mass ratio of 0.55:16.8:13. The zinc solution was added to the benzimidazole solution with zinc-to-benzimidazole molar ratio of 491:375. The reaction was carried out at room temperature under stirring for 2 h. The ZIF-11 crystals were recovered by vacuum filtration, washed with methanol, and activated in vacuum oven at 403 K for 24 h. Particle size distributions of the ZIF-11 crystals are measured by SEM and analyzed by ImageJ (Figs. S2 and S3, and Table S1). The measured powder x-ray diffraction pattern (Fig. S4) was found to be in agreement with the corresponding simulated pattern of ZIF-11. Two identically prepared batches of ZIF-11 crystals with similar crystal size distribution and similar average crystal size (A and B in Fig. S3 and Table S1) were used in this work. Two batches were needed to prepare all studied MMM samples. As shown in this paper later, the corresponding gas intracrystalline diffusivities were found to be the same for both batches.

2.2. 6FDA-DAM synthesis

6FDA-DAM was synthesized according to literature [33]. The dry monomers, 6FDA (dianhydrides, 4,4'-(Hexafluoroisopropylidene) diphthalic anhydride) (BTC) and DAM (diamine diaminomesitylene) (Sigma Aldrich), were further purified via vacuum (100 mTorr) sublimation at 488 K (6FDA) and 373 K (DAM). Reactors were purged with N_2 and propane torched under inert purging prior to the reaction and maintained at 273 K. The purified DAM monomer was dissolved into dehydrated NMP under stirring and inert purging. The 6FDA monomer was then added. After 24 h, beta-picoline was added. Acetic anhydride was added at the complete dissolution of beta-picoline. The 6FDA-DAM was precipitated into methanol and extensively washed with methanol, followed by vacuum drying.

2.3. Mixed-matrix membrane fabrication

Torlon ® 4000T-HV was purchased from Solvay and Matrimid ® 5218 was purchased from Huntsman. The polymers utilized in this paper have different compressive moduli: Torlon (4.5 GPa [24,25]), Matrimid (3.5 GPa [26]), and 6FDA-DAM (1.2 GPa [27]). Chemical structures of these polymers can be seen in Figs. S5–S7, respectively [34–36].

All mixed-matrix membranes are fabricated via the same procedure. 50 mg of dry polymer powder was firstly dissolved in 10 g N-Methyl-2-pyrrolidone (BDH). Upon complete dissolution, 70 mg of ZIF-11 crystals were dispersed in the dilute polymer solution under sonication. After that, 580 mg of dry polymer powder was added. The mixture is then put on a rolling mixer for 72 h.

Prior to membrane fabrication, the membrane dope was degassed overnight. The mixed matrix dense films are then blade-casted in a glove bag filled with nitrogen. The as-cast membranes were slowly dried in the solvent-saturated atmosphere for over 72 h. After complete drying, the mixed-matrix membranes were annealed at 473 K under dynamic vacuum for 24 h. ZIF-11 particles are uniformly distributed in the polymer matrix as shown in Fig. S8.

2.4. Preparation of NMR samples

The ZIF-11 crystals were introduced into 5 mm (thin walled) NMR tubes (Wilmad Labglass, Inc.). The height of beds of ZIF-11 crystals in the tubes was about 20 ± 4 mm. To prepare NMR samples of polymer films and mixed matrix membranes, the films were rolled into densely packed cylinders with the length and diameter of around 30 ± 3 mm and 4 mm, respectively. The cylinders were placed into 5 mm NMR tubes of the same type as those used for crystal powders. Each NMR sample was activated, i.e. made sorbate free, by attaching it to a custom-made vacuum system and heating it slowly under high vacuum up to 423 K. Once the sample had been activated by keeping it under high vacuum overnight at 423 K, sorbate loading was performed. The sorbates used for this study were ^{13}C-labeled ethane (Sigma-Aldrich) and $^{13}C_2$-labeled ethylene (Sigma-Aldrich). The gases were loaded into the NMR samples by freezing the desired mass of each gas into the NMR tubes using liquid nitrogen. Upon loading, the tubes were flame-sealed and detached from the vacuum system. Samples with small gas loadings corresponding to gas pressures less than 1 bar were also loaded by exposing them to the sorbate (ethane or ethylene) at 296 K and desired gas pressure for at least 2 h. The latter time ensured no changes in the

Table 1
Loading pressure and corresponding concentration of ethane or ethylene in the ZIF-11 bed and ZIF-11-based MMM samples at 296 K as measured using NMR signal analysis. Each sample contained a single gas (ethane or ethylene).

Sample	Ethane loading pressure[a], bar	Ethane loading[b], mmol/g	Ethylene loading pressure[a], bar	Ethylene loading[b], mmol/g
ZIF-11 bed	0.8	1.4	0.8	1.2
ZIF-11 bed	2.1	2.0	2.0	1.7
ZIF-11 bed	9.1	3.0	9.0	3.1
ZIF-11/Torlon MMM	0.8	0.15	0.8	0.06
ZIF-11/Torlon MMM	2.1	0.34	2.2	0.40
ZIF-11/Torlon MMM	8.2	1.8	9.1	1.5
ZIF-11/Matrimid MMM	0.8	0.08	0.8	0.07
ZIF-11/Matrimid MMM	8.7	0.62	9.1	1.1
ZIF-11/6FDA-DAM MMM	0.8	0.45	0.8	0.34
ZIF-11/6FDA-DAM MMM	2.3	1.1	2.4	0.85
6FDA-DAM Polymer	0.8	0.20	0.8	0.17

[a] 15% experimental uncertainty.
[b] 25% experimental uncertainty.

amount adsorbed when even longer equilibration times are used, as confirmed based on the measured NMR signal of each gas.

The gas concentrations in the samples were obtained by comparing the gas NMR signal in the studied samples with the NMR signal in the corresponding reference sample containing only bulk gas at a known pressure, in a similar way as discussed in Ref. [37]. An additional procedure was also used for the samples loaded by gas freezing using liquid N_2. In this case, NMR tube with a porous sample was placed upside down into the PFG NMR probe to measure the NMR signal from the gas volume of the tube. In order to prevent the porous sample from falling down a gas-permeable Doty Susceptibility plug (Wilmad Labglass, Inc.) was introduced inside each tube. NMR signal measured for the gas phase of the tube was compared with the signal in the corresponding reference sample containing bulk gas only. Gas concentration inside a porous material was obtained by subtracting the gas amount in the volume of the tube not occupied by the porous material from the total amount of gas in the tube. Table 1 shows the loading pressures and the corresponding sorbate concentrations obtained for each studied sample.

2.5. NMR measurements

Pulsed field gradient NMR diffusion measurements were carried out using a 14 T Avance III spectrometer (Bruker Biospin) and 17.6 T Avance III HD spectrometer (Bruker Biospin). The resonance frequencies for ^{13}C at 14 and 17.6 T were 149.8 MHz and 188.6 MHz, respectively. The corresponding resonance frequencies for ^{1}H at 14 and 17.6 T were 600 MHz and 750 MHz, respectively. Bipolar, trapezoidal-shaped as well as sine-shaped magnetic field gradients with the amplitudes up to 25 T/m and 18 T/m were generated using Diff50 and Diff30 diffusion probes (Bruker BioSpin), respectively. The effective gradient pulse width was 2–2.5 ms. The NMR data reported in this work were measured after keeping the samples at a chosen temperature inside the magnets for a minimum of 1 h to ensure that the sorption equilibrium is reached between the porous material and gas phase of the samples. NMR signal, which is proportional to the total amount of gas in the measured sample volume, was monitored during the measurements that lasted at least several hours at any given temperature. No changes in the signal were observed, indicating that there were no changes in the gas concentration inside the studied porous materials. These observations verified the conditions of sorption equilibrium during our measurements.

The 13-interval PFG NMR pulse sequence with bipolar gradients [38] and added eddy current delay was used in the diffusion measurements. The measurements were performed at different diffusion times between around 10 and 270 ms. The time delay between the first and second $\pi/2$ radiofrequency pulses of the sequence was 8.5 ms and 3.5 ms, respectively, for ^{13}C and ^{1}H. The gas self-diffusivities were obtained from the PFG NMR attenuation curves, i.e. the dependencies of the intensity of the measured PFG NMR signal on the magnetic field gradient amplitude (g) measured under the conditions when all other parameters are held constant. Signal intensities represent the area under the spectra recorded by the PFG NMR sequence. The ^{13}C NMR spectra of ethane and ethylene were single lines at about 4.0 and 120.5 ppm, respectively. The ^{1}H NMR spectra of ethane and ethylene were also single lines at different chemical shifts of around 1.8 and 6.3 ppm, respectively. PFG NMR attenuation curves measured for any fixed diffusion time t are expected to obey a simple monoexponential relation if all molecules of the same type diffuse in the sample with the same self-diffusion coefficient (D) [39–42].

$$\Psi = \frac{S(g)}{S(g \approx 0)} = \exp(-Dq^2t) \tag{1}$$

where Ψ is the PFG NMR signal attenuation, S is the PFG NMR signal intensity, and $q = 2\gamma g\delta$, where δ is the gradient pulse duration and γ is the gyromagnetic ratio. For normal 3-dimensional diffusion, the mean square displacement (MSD) can be calculated using the Einstein relation

$$<r^2> = 6Dt. \tag{2}$$

If there are two molecular ensembles with different self-diffusivities, the attenuation curves can be presented as follows [39,40].

$$\Psi = \frac{S(g)}{S(g \approx 0)} = \sum_{i}^{n=2} p_i \exp(-D_i q^2 t), \tag{3}$$

where D_i and p_i are, respectively, the self-diffusivity and phase fraction of ensemble i ($i = 1$ or 2).

Most of the PFG NMR attenuation curves reported in this work were measured at 17.6 T using ^{13}C nuclei. ^{13}C PFG NMR was used instead of more traditional ^{1}H PFG NMR to reduce the expected signal loss due to T_2 NMR relaxation process, which is much faster for ^{1}H than for ^{13}C in the samples studied in this work (Tables S2 and S3). In order to confirm the lack of magnetic susceptibility distortions and/or any other measurement artifacts, complementary diffusion measurements were performed with selected samples under the same or similar measurement conditions using ^{1}H nuclei at 17.6 T or ^{13}C nuclei at a lower field of 14 T. The observed coincidence of the results obtained from the latter measurements with the corresponding data measured with the same samples by ^{13}C PFG NMR at 17.6 T confirmed the absence of any measurement artifacts under our experimental conditions.

The uncertainty of the diffusivities reported in the paper is based on the reproducibility of the diffusion data measured with several identically prepared (but different) NMR samples. The uncertainty of the diffusivities is also determined by the reproducibility of the results obtained for the same samples by using different nuclei types (^{13}C and ^{1}H) and or different magnetic field strengths (17.6 and 14 T).

In addition to diffusion measurements, the 13-interval PFG NMR sequence was also applied to estimate transverse (T_2) and longitudinal (T_1) NMR relaxation times. In the T_2 NMR relaxation measurements using this sequence, the time delays between the first and second $\pi/2$ radiofrequency pulses and between the third $\pi/2$ radiofrequency pulse and the beginning of the eddy current delay were changed while keeping all other time delays constant. In the T_1 NMR relaxation measurements, the time delay between the second and third $\pi/2$ radiofrequency pulses was changed while keeping all other time delays constant. It was verified that there was no change in the measured signal due to gas diffusion inside ZIF-11 crystals or MMMs under the conditions of the relaxation measurements. In these measurements, all signal from the gas volume of the samples was completely attenuated away by the applied gradients. Hence, the measured relaxation times correspond to gas molecules located inside porous materials. The measured T_1 and T_2 NMR relaxation times are presented in Tables S2 and S3. No experimental evidence was observed for an existence of distributions over T_1 and T_2 relaxation times in the studied samples.

3. Results and discussion

Fig. 1 shows examples of the PFG NMR attenuation curves measured for ethane diffusion at 296 K in ZIF-11 based MMMs and ZIF-11 crystal beds at the low ethane loading corresponding to the ethane loading pressure of 0.8 bar. Here and later, ZIF-11 crystals from the same batch were used when comparing diffusion data on the same graph for an MMM and the corresponding crystal bed. The data in each graph were obtained for the same gas loading pressure for each MMM/crystal bed pair resulting in the same intra-ZIF concentration in each particular pair. Examples of the PFG NMR attenuation curves at 296 K and the highest ethane loadings used in this study are presented in Fig. S9. It should be noted that, for ZIF-11/Torlon and ZIF-11/Matrimid MMMs, the highest ethane loadings correspond to ethane loading pressure of around 9 bar. However, in the case of ZIF-11/6FDA-DAM MMM, the largest loading pressure was limited to only 2.3 bar to avoid plasticization effects at higher sorbate loadings. Such plasticization effects were previously discussed in our recent paper [23] for the case of loading this MMM with ethylene. For ZIF-11/Torlon MMM the PFG NMR measurements of ethane diffusion were also performed for an additional, intermediate loading at 296 K (Fig. S10). The intermediate loading of ethane for this MMM corresponds to the ethane loading pressure of 2.1 bar. The corresponding PFG NMR data for ethylene diffusion at 296 K for the same MMMs and ZIF-11 beds have already been reported in Ref. [23].

The PFG NMR attenuation curves for ZIF-11/Torlon (Figs. 1A, S9A, S10) and ZIF-11/Matrimid (Figs. 1B and S9B) MMMs are observed to be in agreement with Eq. (1), i.e. show a monoexponential behavior in the presentation of our figures. This indicates that for each sample at any measured diffusion time there is a single ethane self-diffusivity. The attenuation curves measured for these MMMs can be attributed to the diffusion inside the crystals of ZIF-11 dispersed in the MMMs, as the intra-polymer diffusion does not contribute to the measured attenuation curves due to a combination of short T_2 NMR relaxation times and low gas concentration in the polymer matrix. This was confirmed by the absence of a measurable PFG NMR signal of ethane molecules in the pure polymer films at the same or comparable ethane loading pressures. It is important to note that the PFG NMR signal of ethane from the gas phase of the samples was already fully attenuated at the smallest gradient amplitude used. The ^{13}C PFG NMR attenuation curves measured for ethane diffusion in ZIF-11/6FDA-DAM MMM (Figs. 1C and S9C) deviate from the monoexponential behavior predicted by Eq. (1). For this MMM, the ethane diffusion inside the polymer matrix contributes to the attenuation curves. Such contribution is expected based on our previous ^{13}C PFG NMR measurements of ethane diffusion in a different MMM containing 6FDA-DAM polymer [28,29]. Indeed, the T_2 ^{13}C NMR relaxation time of ethane in the 6FDA-DAM polymer was observed to be sufficiently large (Table S2) [29] for the measurements by ^{13}C PFG NMR. Hence, the results of the ^{13}C PFG NMR measurements of ZIF-11/

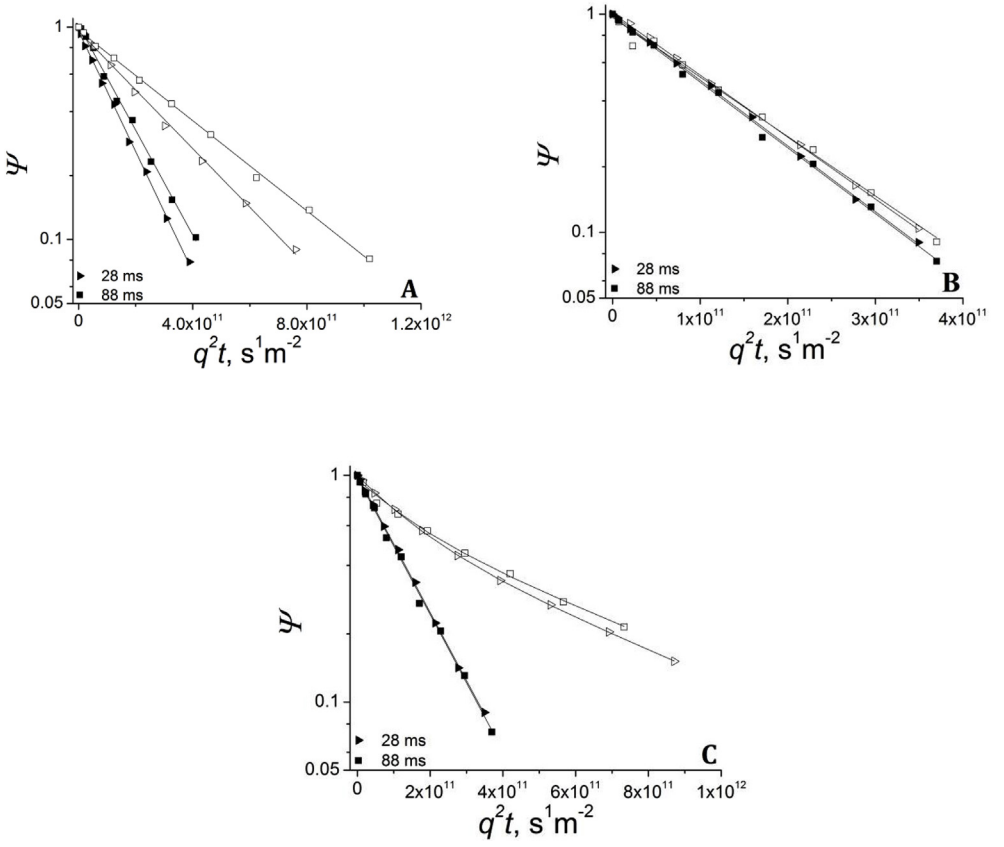

Fig. 1. ^{13}C PFG NMR attenuation curves measured for intra-ZIF diffusion of ethane at a loading pressure of 0.8 bar at 296 K in a bed of ZIF-11 crystals (filled symbols) and ZIF-11 based MMMs (hollow symbols). The MMMs were prepared using polymers Torlon (A), Matrimid (B), and 6FDA-DAM (C). The measurements were performed at different diffusion times shown in the figure. The solid lines represent the results of least-square fitting using Eq. (1) for monoexponential curves and Eq. (3) for non-monoexponential curves in C.

Table 2
PFG NMR data for intra-ZIF diffusion of ethane measured at 296 K for ZIF-11/Torlon MMM and the corresponding ZIF-11 bed for several matching ethane loading pressures and diffusion times. Also shown are the root MSD values calculated using Eq. (2).

Loading Pressure (bed)[a], bar	Loading Pressure (MMM)[a], bar	Diffusion Time, ms	D(bed), $10^{-12}\frac{m^2}{s}$	Root MSD (bed), μm	D(MMM), $10^{-12}\frac{m^2}{s}$	Root MSD (MMM), μm
0.8	0.8	28	6.5 ± 0.6	1.0 ± 0.1	3.2 ± 0.3	0.72 ± 0.04
0.8	0.8	88	5.7 ± 0.6	1.7 ± 0.1	2.5 ± 0.3	1.1 ± 0.1
2.1	2.1	28	5.6 ± 0.5	0.96 ± 0.05	3.2 ± 0.3	0.72 ± 0.04
2.1	2.1	88	5.2 ± 0.5	1.7 ± 0.1	2.7 ± 0.3	1.1 ± 0.1
2.1	2.1	268	4.6 ± 0.5	2.7 ± 0.1	2.0 ± 0.2	1.8 ± 0.1
9.1	8.2	28	2.7 ± 0.2	0.66 ± 0.02	2.4 ± 0.2	0.63 ± 0.03
9.1	8.2	88	2.4 ± 0.2	1.1 ± 0.1	2.1 ± 0.2	1.1 ± 0.1
9.1	8.2	268	2.1 ± 0.2	1.9 ± 0.1	1.7 ± 0.2	1.6 ± 0.1

[a] Approximately 15% uncertainty.

Table 3
PFG NMR data for intra-ZIF diffusion of ethane measured at 296 K for ZIF-11/Matrimid MMM and the corresponding ZIF-11 bed for several matching ethane loading pressures and diffusion times. Also shown are the root MSD values calculated using Eq. (2).

Loading Pressure (bed)[a], bar	Loading Pressure (MMM)[a], bar	Diffusion Time, ms	D(bed), $10^{-12}\frac{m^2}{s}$	Root MSD (bed), μm	D(MMM), $10^{-12}\frac{m^2}{s}$	Root MSD, (MMM), μm
0.8	0.8	28	6.9 ± 0.7	1.1 ± 0.1	6.5 ± 0.6	1.0 ± 0.1
0.8	0.8	88	6.9 ± 0.7	1.9 ± 0.1	6.3 ± 0.6	1.8 ± 0.1
9.1	8.7	28	2.9 ± 0.3	0.7 ± .05	3.3 ± 0.3	0.74 ± 0.05
9.1	8.7	88	2.6 ± 0.3	1.2 ± 0.1	2.5 ± 0.3	1.2 ± 0.1
9.1	8.7	268	2.6 ± 0.3	2.0 ± 0.1	2.8 ± 0.3	2.1 ± 0.1

[a] Approximately 15% uncertainty.

Table 4
PFG NMR data for intra-ZIF and intra-polymer diffusion of ethane measured at 296 K for ZIF-11/6FDA-DAM MMM and the corresponding intra-ZIF diffusivities in ZIF-11 bed for several matching ethane loading pressures and diffusion times. Also shown are the root MSD values calculated using Eq. (2).

Loading Pressure (bed)[a], bar	Loading Pressure (MMM)[a], bar	Diffusion Time, ms	D(bed), $10^{-12}\frac{m^2}{s}$	Root MSD (bed), μm	D_1, $10^{-12}\frac{m^2}{s}$ Polymer ensemble	D_2, $10^{-12}\frac{m^2}{s}$ ZIF ensemble	P_1	P_2	Root MSD (MMM) 1, μm	Root MSD (MMM) 2, μm
0.8	0.8	28	6.9 ± 0.7	1.1 ± 0.1	1.0 ± 0.3	6.9 ± 0.7	0.41	0.59	0.47 ± 0.05	1.1 ± 0.1
0.8	0.8	88	6.9 ± 0.7	1.9 ± 0.1	1.1 ± 0.3	6.8 ± 0.7	0.50	0.50	0.77 ± 0.10	1.9 ± 0.1
2.1	2.3	28	5.3 ± 0.5	0.93 ± .04	1.1 ± 0.2	5.6 ± 0.6	0.34	0.66	0.42 ± 0.04	0.96 ± 0.05
2.1	2.3	88	5.3 ± 0.5	1.7 ± 0.1	1.1 ± 0.2	5.5 ± 0.6	0.40	0.60	0.89 ± 0.10	1.9 ± 0.1
2.1	2.3	268	–	–	1.1 ± 0.2	5.4 ± 0.6	0.36	0.64	1.3 ± 0.1	3.0 ± 0.2

[a] Approximately 15% uncertainty.

6FDA-DAM MMM exhibit the existence of two ethane ensembles. The first one corresponds to ethane diffusion in the polymer matrix, and the second corresponds to ethane diffusion inside the ZIF crystals. The PFG NMR attenuation curves measured in ZIF-11/6FDA-DAM MMM for different diffusion times were found to be almost identical in the presentation of Figs. 1C and S9C indicating that under our measurement conditions there was no significant exchange between the two ensembles. Therefore, Eq. (3), which assumes the existence of two non-exchanging molecular ensembles with different diffusivities, was applied to fit the PFG NMR attenuation curves for this MMM. It is important to note that when a significant exchange between different molecular ensembles is expected, i.e. for diffusion times larger than those used in this study, a diffusion exchange model can be used to quantify the diffusion process [43,44]. For ZIF-11/Torlon and ZIF-11/Matrimid MMMs Eq. (1) was used to fit the PFG NMR attenuation curves. The resulting best fit data are shown in Tables 2, 3, and 4 for the MMMs prepared with Torlon, Matrimid, and 6FDA-DAM, respectively. These tables also show the corresponding data for the respective ZIF-11 beds.

The two ethane ensembles in the MMM with 6FDA-DAM were assigned to intra-ZIF and intra-polymer ensembles based on the comparison of the diffusivities of these ensembles in Table 4 with the ethane self-diffusivity in a 6FDA-DAM film reported in Ref. [29] and Fig. S11 for the high and low ethane loading pressures, respectively. The attenuation curves for the 6FDA-DAM polymer at the low ethane loading pressure exhibit the expected monoexponential behavior, indicating that all ethane molecules diffuse in the polymer with a single diffusivity. The coincidence of the attenuation curves in Fig. S11 measured for different diffusion times shows that this diffusivity does not depend on diffusion time in the measured range. The intra-polymer diffusivity of ethane was found to be equal to $(1.1 \pm 0.1) \times 10^{-12}\,m^2/s$ by least square fitting of the attenuation data in Fig. S11 using Eq. (1). Comparison of this diffusivity to that in Table 4 shows no change in the intra-polymer diffusivity of ethane due to the formation of ZIF-11/6FDA-DAM MMM. In contrast, the intra-polymer diffusivity of ethylene was found to be slightly reduced by the formation of the MMM [23]. The latter effect was attributed to the polymer chain rigidification induced by the MMM formation.

Diffusion time independent self-diffusivities of ethane were observed, within uncertainty, for intra-ZIF diffusion in ZIF-11/6FDA-DAM and ZIF-11/Matrimid MMMs, as well as in the corresponding beds of ZIF-11 crystals (Tables 3, 4). At the same time, the intra-ZIF self-diffusivity of ethane in ZIF-11/Torlon MMM and the corresponding batch of ZIF-11 crystals exhibits some gradual decrease with increasing diffusion time (Table 2). The same trend of decreasing diffusivity with increasing diffusion time was previously reported for ZIF-11 beds loaded with different sorbates, methane and carbon dioxide [45]. Analysis of this dependence using the approach presented by Mitra

et al. [46–49] revealed consistency with the case of reflective external crystal surface when sufficiently short diffusion times are used in the measurements. The small diffusivity decrease with increasing time observed in ZIF-11/Torlon MMM and the corresponding ZIF-11 bed (Table 2) can also be attributed to the effects at the external crystal surface based on the similarity between the root MSD values and the average crystal size of 3.1 μm (Table S1). A relatively broad distribution of ZIF-11 crystal sizes (Fig. S3) prevented us from performing quantitative analysis based on the formalism of Mitra et al. as discussed above. The data in Table 2 show that the extent of the diffusivity changes due to identical changes of the diffusion time are quite similar for the MMM and crystal bed. This is consistent with the lack of formation of any defects in ZIF-11 crystals or a reduction in the crystal size by embedding the crystals in the Torlon polymer. At the same time, for the other two MMMs and their respective ZIF-11 beds, a larger average ZIF-11 crystal size (4.5 μm from Table S1) was the reason for an absence of time dependence of intra-ZIF diffusivity, within uncertainty. Furthermore, it can be seen in Tables 2, 3, and 4, that the intra-ZIF diffusivities in ZIF-11 beds are the same, within uncertainty, for the two different ZIF-11 batches measured for the smallest diffusion times under the same or similar conditions. This observation provides an additional evidence of the reproducibility of the reported intra-ZIF diffusivities in different ZIF-11 batches when the influence of the external surface effects on these diffusivities is small or nonexistent.

The results in Table 2 show a smaller intra-ZIF diffusivity of ethane in ZIF-11/Torlon MMM compared to the intra-ZIF diffusivity in the corresponding ZIF-11 bed under identical measurement conditions for the smallest and intermediate ethane loadings. At the same time, these diffusivities are the same within uncertainty at the largest ethane loading. The results in Tables 3 and 4 indicate that the intra-ZIF diffusivities of ethane in ZIF-11/Matrimid and ZIF-11/6FDA-DAM are the same, within uncertainty, as those in their respective ZIF-11 beds under identical measurement conditions for all studied ethane loadings. The observed relationship between the intra-ZIF diffusivities in the MMMs and in the corresponding ZIF-11 beds for ethane are qualitatively the same as those reported previously for ethylene [23]. Quantitatively, the intra-ZIF diffusivities in the beds and MMMs can be compared to one another as ratios. The ratios of intra-ZIF diffusivity in ZIF-11/polymer MMMs to intra-ZIF diffusivity in ZIF-11 beds at 296 K for ethane (this work) and ethylene (from Ref. [23]) for different matching loading pressures are shown in Fig. 2. For the samples that showed a time-dependence of the measured diffusivity (i.e., ZIF-11/Torlon MMM and the corresponding ZIF-11 bed), the ratios were calculated using the diffusivities measured at the shortest diffusion times when any effects at the external surface of ZIF-11 crystals on the measured self-diffusivity

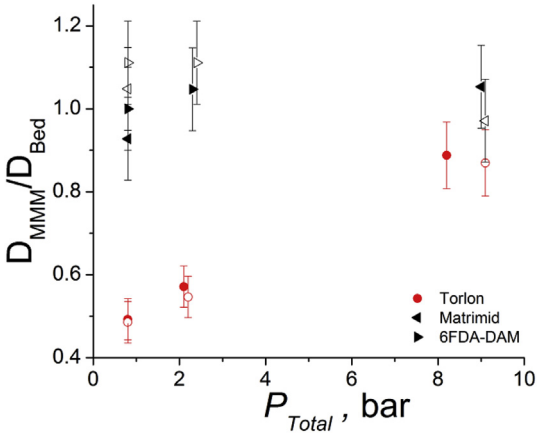

Fig. 2. Ratios of intra-ZIF self-diffusivities of ethane (filled symbols) and ethylene (hollow symbols) in ZIF-11 based MMMs to ZIF-11 as a packed crystal bed for different sorbate loading pressures at 296 K.

can be considered to be negligibly small. For the remaining samples that showed, within uncertainty, no diffusivity time-dependence (i.e., MMMs prepared with Matrimid and 6FDA-DAM and the corresponding ZIF-11 beds), the average self-diffusivity over all diffusion times was used to calculate the ratios. The diffusivity reduction in ZIF-11/Torlon MMM in comparison to the bed can be seen in Fig. 2 to be similar or even the same, within experimental uncertainty, for both ethane and ethylene at the lowest and intermediate sorbate loadings, indicating this reduction is independent of the studied sorbate. In agreement with our previous work [23], this reduction in the diffusivity is tentatively attributed to a reduced framework flexibility of ZIF-11 crystals due to the confinement in Torlon. As we previously reported, the higher bulk modulus of Torlon (4.5 GPa [24,25]) in comparison with those of Matrimid (3.5 GPa [26]) and 6FDA-DAM (1.2 GPa [27]) may be the primary reason for the lack of a similar confinement effect on diffusion in the latter two MMMs. In addition, possible differences in the ZIF-11/polymer adhesion for different studied polymers may also play a role in the observed confinement effect.

Fig. 2 also shows that for the largest sorbate loading pressures used, this intra-ZIF diffusivity in ZIF-11 bed and ZIF-11/Torlon MMM are the same, within uncertainty, for both sorbates, i.e. the diffusivity ratios are around 1. As previously discussed for the case of ethylene diffusion [23], the observed increase in the diffusivity ratio in Fig. 2 with increasing loading pressure can be tentatively explained as follows. It is possible that at high sorbate loadings ZIF-11 framework flexibility is partially restricted by adsorbed molecules. For example, linker reorientation might be restricted if guest molecules are hindering such reorientation movements due to either a specific guest-linker interaction or a reduction in the available free volume caused by a high concentration of guest molecules. It is also possible that the sorbate molecules present in Torlon cause some plasticization effects in the polymer at the largest sorbate loading pressures used in this study. Such plasticization effects can reduce the extent of confinement of ZIF-11 crystals in ZIF-11/Torlon MMM.

The data in Fig. 2 indicate that the ratio of the intracrystalline self-diffusivities for ethane and ethylene in the studied MMMs (i.e. ethane/ethylene intra-ZIF diffusion selectivity) is not changed appreciably in comparison to unconfined ZIF-11 crystals in a crystal bed. The corresponding diffusion selectivity values for the MMMs are shown in Table S4. These values show that larger ethane molecules diffuse faster than smaller ethylene molecules inside ZIF-11 crystals. Such anomalous relationship between the molecular size and intra-ZIF diffusivity is reported and discussed in detail in our previous work for unconfined ZIF-11 crystals [50]. This anomalous relationship is tentatively attributed to the existence of ZIF-11/ethylene interactions, which decrease the rate of molecular diffusion inside ZIF-11 crystals. The main consequence of such interactions can be a reduction in the linker flexibility resulting in a reduced maximum and/or effective aperture size in ZIF-11 crystals. This aperture reduction is expected to slow down diffusion of both ethane and ethylene, in agreement with our diffusion data.

To investigate further the effect of ZIF-11 crystal confinement in Torlon on intra-ZIF diffusion, PFG NMR was applied to measure temperature dependencies of ethane and ethylene intra-ZIF self-diffusion coefficients in ZIF-11/Torlon MMM. Examples of the PFG NMR attenuation curves measured at selected temperatures for intra-ZIF ethane and ethylene self-diffusion in this MMM are shown in Fig. S12. This figure also shows, for comparison, the corresponding attenuation curves in ZIF-11 beds, which were previously reported in Ref. [50]. The result of least-squares fitting of the attenuation curves in Fig. S12 using Eq. (1) are presented in Tables S5 and S6. These tables also show the root MSD values calculated using Eq. (2). ZIF-11/Torlon MMM samples with different total amount of gas (ethane or ethylene) in the sealed NMR tubes were prepared and measured to ensure an availability of the diffusion data for the same or similar intra-ZIF sorbate concentrations under the measurements conditions at different temperatures. The diffusion measurements were also performed at different diffusion

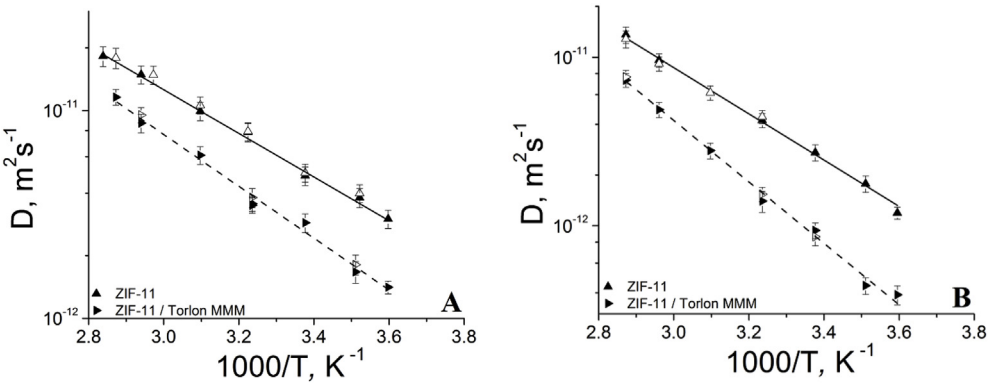

Fig. 3. Temperature dependence of sorbate self-diffusion coefficients measured by PFG NMR for the observation times pertaining to the same or similar MSD for ethane (A) or ethylene (B) loaded in ZIF-11 bed or ZIF-11/Torlon MMM. Measurements were performed using both ^{1}H (filled symbols) and ^{13}C (hollow symbols) nuclei. The intra-ZIF gas loading was around 2 mmol/g at all temperatures.

Table 5
Intra-ZIF diffusivities of ethane measured by ^{1}H and ^{13}C PFG NMR for ZIF-11/Torlon MMM at different temperatures while keeping the root MSD value the same or similar. The intra-ZIF gas loading was around 2 mmol/g at all temperatures.

Loading Pressure at 296 K (MMM)[a], bar	Diffusion Time, ms	Nuclei type	Temperature, K	D, $10^{-12}\frac{m^2}{s}$	Root MSD (MMM), μm
2.1	179	^{1}H	278	1.4 ± 0.2	1.2 ± 0.1
2.1	149	^{1}H	284	1.7 ± 0.2	1.2 ± 0.1
2.1	148	^{13}C	284	1.8 ± 0.2	1.3 ± 0.1
2.1	89	^{1}H	296	2.9 ± 0.3	1.2 ± 0.1
2.1	79	^{1}H	309	3.6 ± 0.3	1.3 ± 0.1
2.1	78	^{13}C	309	3.8 ± 0.3	1.3 ± 0.1
4.4	79	^{1}H	309	3.5 ± 0.3	1.3 ± 0.1
4.4	59	^{1}H	323	6.1 ± 0.6	1.5 ± 0.1
4.4	39	^{1}H	340	8.7 ± 0.8	1.4 ± 0.1
4.4	38	^{13}C[b]	340	9.5 ± 0.9	1.5 ± 0.1
4.4	39	^{1}H	348	10.1 ± 1.0	1.5 ± 0.1

[a] 15% experimental uncertainty.
[b] Measured at 14 T (all other data measured at 17.6 T).

times to ensure that for each sorbate the self-diffusivities at different temperatures can be compared for the same or similar values of root MSDs significantly smaller than the mean crystal size in the MMM. This was done to avoid or minimize distortions of the diffusivity temperature dependencies by crystal boundary effects. Fig. 3 and Tables 5, 6 present the diffusion data for ZIF-11/Torlon MMM that, for each sorbate, correspond to the same or similar intra-ZIF concentration and root MSDs at different temperatures. For comparison, this figure and tables also show the corresponding diffusion data for ZIF-11 beds from Ref. [50]. It is seen in Fig. 3 and Tables 5, 6 that, within experimental uncertainty, there is no difference between the measured self-diffusivities when using different types of nuclei (^{1}H and ^{13}C) and otherwise the same or similar conditions. This observation indicates the absence of any types of measurement artifacts in the reported diffusivities.

The data in Fig. 3 show that for both ethane and ethylene the diffusivity temperature dependence can be described using the Arrhenius law

$$D(T) = D_0 \exp\left(-\frac{E_a}{RT}\right) \quad (4)$$

where E_a is the activation energy of diffusion and D_0 is the pre-exponential factor. Least-squares fitting of the data for ZIF-11/Torlon MMM in Fig. 3 using Eq. (4) resulted in diffusion activation energies of 23.8 ± 3.0 kJ/mol and 34.9 ± 4.0 kJ/mol for ethane and ethylene, respectively. For ethylene, the activation energy of diffusion in ZIF-11/Torlon MMM (34.9 kJ/mol) was found to be somewhat larger than the corresponding activation energy of diffusion in ZIF-11 bed (26.3 kJ/mol [50]). For ethane, our data do not rule out that the activation energy of diffusion in ZIF-11/Torlon MMM (23.8 kJ/mol) is also slightly larger than that in the ZIF-11 bed (20.0 kJ/mol [50]). However, the experimental uncertainty prevents us from making a definitive conclusion regarding the relationship of the activation energies for ethane. The observation of an increase in the activation energy for intra-ZIF diffusion of ethylene when ZIF-11 is confined in the Torlon polymer is consistent with a reduced framework flexibility of the confined ZIF-11 crystals. Such reduced framework flexibility of ZIF-11 may decrease the extent of fluctuations in the aperture size at any given temperature while keeping the effective (average) pore aperture size the same or even making it smaller. This effect of the flexibility reduction on the diffusion activation energy can be stronger for ethylene than for ethane because of a stronger interaction of ethylene molecules with the ZIF-11 framework, as discussed in Ref. [50].

Table 6
Intra-ZIF diffusivities of ethylene measured by ^{1}H and ^{13}C PFG NMR for ZIF-11/Torlon MMM at different temperatures while keeping the root MSD value the same or similar. The intra-ZIF gas loading was around 2 mmol/g at all temperatures.

Loading Pressure at 296 K (MMM)[a], bar	Diffusion Time, ms	Nuclei type	Temperature, K	D, $10^{-12}\frac{m^2}{s}$	Root MSD (MMM), μm
2.2	179	^{1}H	278	0.39 ± 0.05	0.65 ± 0.05
2.2	149	^{1}H	285	0.44 ± 0.05	0.63 ± 0.04
2.2	89	^{1}H	296	0.93 ± 0.1	0.71 ± 0.04
2.2	88	^{13}C	296	0.86 ± 0.09	0.67 ± 0.04
3.0	89	^{1}H	309	1.4 ± 0.2	0.87 ± 0.05
3.0	88	^{13}C[b]	309	1.5 ± 0.2	0.90 ± 0.05
3.0	49	^{1}H	323	2.8 ± 0.3	0.91 ± 0.05
4.1	19	^{1}H	338	4.9 ± 0.5	0.75 ± 0.04
4.1	19	^{1}H	348	7.3 ± 0.7	0.91 ± 0.05
4.1	19	^{13}C[b]	348	7.6 ± 0.7	0.93 ± 0.05

[a] 15% experimental uncertainty.
[b] Measured at 14 T (all other data measured at 17.6 T).

4. Conclusion

Multinuclear PFG NMR was used to measure intra-ZIF diffusivities of ethane in ZIF-11 based MMMs at different ethane concentrations, different diffusion times, and, for selected samples, at different temperatures. The measured ethane diffusivities were compared with the corresponding diffusivities in ZIF-11 crystal beds. In a complete analogy with the report of a reduced intra-ZIF diffusivity of ethylene inside ZIF-11/Torlon MMM in comparison to that in ZIF-11 bed at 296 K in our previous short paper [23], comparable intra-ZIF diffusivity reduction was also observed here for ethane. In the current work, PFG NMR was used to measure temperature dependencies of intra-ZIF diffusivities in ZIF-11/Torlon MMM for both ethane and ethylene. These measurements resulted in the observation of a higher activation energy of intra-ZIF diffusion of ethylene in ZIF-11/Torlon MMM than in the corresponding ZIF-11 bed. At the same time, the corresponding activation energies for ethane were found to be the same, within uncertainty. A reduced framework flexibility of ZIF-11 crystals confined in Torlon is the likely reason for lower intra-ZIF diffusivities in ZIF-11/Torlon MMM than in the ZIF-11 beds for both studied sorbates. This reduction of the framework flexibility of ZIF-11 may decrease the extent of fluctuations in the pore aperture size and/or make the effective (average) aperture smaller. In contrast, no influence of the confinement of ZIF-11 crystals on the intra-ZIF diffusion was observed for the other two studied MMMs formed with Matrimid and 6FDA-DAM. The lack of such influence was attributed to the lower bulk moduli of Matrimid and 6FDA-DAM in comparison to that of Torlon and possible differences in the ZIF-11/polymer adhesion for different studied polymers. For selected matching experimental conditions, the PFG NMR diffusion measurements were performed using different nuclei types (^{13}C and ^{1}H) and different magnetic field strengths (14 T or 17.6 T). The diffusion data was observed to be independent, within uncertainty, of the field and nuclei type, which rules out any potential measurement artifacts in our data. The results reported in this work point out at a complexity of the diffusion behavior that may arise due to confinement of MOF crystals in polymers to form MMMs. Such complexities open the door to a variety of MOF/polymer combinations which may prove ideal for particular challenging gas separations.

Acknowledgments

We are grateful for the financial support of this work by NSF (CBET awards No. 1510411 and No. 1510442). A portion of this work was performed in the McKnight Brain Institute at the National High Magnetic Field Laboratory's AMRIS Facility, which is supported by National Science Foundation Cooperative Agreement No. DMR-1157490 and the State of Florida. This work was supported in part by an NIH award, S10RR031637, for magnetic resonance instrumentation. The authors appreciate Dr. Christian Chmelik for his useful comments. The authors thank Dr. Brian Pimentel for the schematic of ZIF-11.

Appendix A. Supplementary data

Supplementary data to this article can be found online at https://doi.org/10.1016/j.memsci.2019.117440.

References

[1] H. Yehia, T.J. Pisklak, J. Ferraris, K. Balkus, I.H. Musselman, Methane facilitated transport using copper(II) biphenyl dicarboxylatetriethylenediamine/poly(3-acetoxyethylthiophene) mixed matrix membranes, Polym. Prepr. 45 (2004) 35–36.
[2] T. Rodenas, M.v. Dalen, E. García-Pérez, P. Serra-Crespo, B. Zornoza, F. Kapteijn, J. Gascon, Visualizing MOF mixed matrix membranes at the nanoscale: towards structure-performance relationships in CO_2/CH_4 separation over NH_2-MIL-53(Al)@Pl, Adv. Funct. Mater. 24 (2014) 249–256.
[3] M.J.C. Ordoñez, K.J.B. Jr., J.P. Ferraris, I.H. Musselman, Molecular sieving realized with ZIF-8/Matrimid® mixed-matrix membranes, J. Membr. Sci. 361 (2010) 28–37.
[4] G. Yilmaz, S. Keskin, Predicting the performance of zeolite imidazolate framework/polymer mixed matrix membranes for CO_2, CH_4, and H_2 separations using molecular simulations, Ind. Eng. Chem. Res. 51 (2012) 14218–14228.
[5] C. Zhang, Y. Dai, J.R. Johnson, O. Karvan, W.J. Koros, High perfromance ZIF-8/6FDA-DAM mixed matrix membrane for propylene/propane separations, J. Membr. Sci. 389 (2012) 34–42.
[6] Y. Zhang, I.H. Musselman, J.P. Ferraris, K.J. B Jr., Gas permeability properties of Matrimid® membranes containing the metal-organic framework Cu-BPY-HFS, J. Membr. Sci. 313 (2008) 170–181.
[7] E.V. Perez, K.J. B Jr., J.P. Ferraris, I.H. Musselman, Mixed-matrix membranes containing MOF-5 for gas separations, J. Membr. Sci. 328 (2009) 165–173.
[8] B.R. Pimentel, A. Parulkar, E.-k. Zhou, N.A. Brunelli, R.P. Lively, Zeolitic imidazolate frameworks: next-generation materials for energy-efficient gas separations, ChemSusChem 7 (2014) 3202–3240.
[9] B. Zornoza, B. Seoane, J.M. Zamaro, C. Téllez, J. Coronas, Combination of MOFs and zeolites for mixed-matrix membranes, ChemPhysChem 12 (2011) 2781–2785.
[10] A. Car, C. Stropnik, K.-V. Peinemann, Hybrid membrane materials with different metal-organic frameworks (MOFs) for gas separation, Desalination 200 (2006) 424–426.
[11] N.A.H.M. Nordin, A.F. Ismail, A. Mustafa, R.S. Murali, T. Matsuura, The impact of ZIF-8 particle size and heat treatment on CO_2/CH_4 separation using asymmetric mixed matrix membrane, RSC Adv. 4 (2014) 52530–52541.
[12] T.-H. Bae, J.S. Lee, W. Qiu, W.J. Koros, C.W. Jones, S. Nair, A high-performance gas-separation membrane containing submicrometer-sized metal-organic framwork crystals, Angew. Chem. Int. Ed. 49 (2010) 9863–9866.
[13] L. Diestel, N. Wang, B. Schwiedland, F. Steinbach, U. Giese, J. Caro, MOF based MMMs with enhanced selectivity due to hindered linker distortion, J. Membr. Sci. 492 (2015) 181–186.
[14] M.S. Boroglu, A.B. Yumru, Gas separation performance of 6FDA-DAM-ZIF-11 mixed-matrix membranes for H_2/CH_4 and CO_2/CH_4 separation, Separ. Purif. Technol. 173 (2017) 269–279.
[15] K. Díaz, M. López-González, L.F.d. Castillo, E. Riande, Effect of zeolitic imidazolate frameworks on the gas transport performance of ZIF8-poly (1,4-phenylene ether-ether-sulfone) hybrid membranes, J. Membr. Sci. 383 (2011) 206–213.
[16] H. Bux, C. Chmelik, R. Krishna, J. Caro, Ethene/ethane separation by the MOF membrane ZIF-8: molecular correlation of permeation, adsorption, diffusion, J. Membr. Sci. 369 (2011) 284–289.
[17] J. Sánchez-Laínez, B. Zornoza, Á. Mayoral, Á. Berenguer-Murcia, Diego Cazorla-Amorós, C. Téllez, J. Coronas, Beyond the H_2/CO_2 upper bound: one-step crystallization and separation of nano-sized ZIF-11 by centrifugation and its application in mixed matrix membranes, J. Mater. Chem. A 3 (2015) 6549–6556.
[18] T. Li, Y. Pan, K.-V. Peinemann, Z. Lai, Carbon dioxide selective mixed matrix composite membrane containing ZIF-7 nano-fillers, J. Membr. Sci. 425–426 (2013) 235–242.
[19] K.S. Park, Z. Ni, A.P. Côté, J.Y. Choi, R. Huang, F.J. Uribe-Romo, H.K. Chae, M. O'Keeffe, O.M. Yaghi, Exceptional chemical and thermal stability of zeolitic imidazolate frameworks, Proc. Natl. Acad. Sci. 103 (2006) 10186–10191.
[20] B. Chen, Z. Yang, Y. Zhu, Y. Xia, Zeolitic imidazoleate framework materials: recent progress in synthesis and applications, J. Mater. Chem. A 2 (2014) 16811–16831.
[21] M. He, J. Yao, Q. Liu, Z. Zhong, H. Wang, Toluene-assisted synthesis of RHO-type zeolitic imidazolate frameworks: synthesis and formation mechanism of ZIF-11 and ZIF-12, Dalton Trans. 42 (2013) 16608–16613.
[22] E.L. First, C.A. Floudas, MOFomics: computational pore characterization of metal-organic frameworks, Microporous Mesoporous Mater. 165 (2013) 32–39.
[23] E.M. Forman, A. Baniani, L. Fan, K.J. Ziegler, E. Zhou, F. Zhang, R.P. Lively, S. Vasenkov, Ethylene diffusion in crystals of zeolitic imidazole Framework-11 embedded in polymers to form mixed-matrix membranes, Microporous Mesoporous Mater. 274 (2019) 163–170.
[24] S.E. Basler, J. Traxler, R. Müller, G.H.v. Lenthe, Peri-implant bone microstructure determines dynamic implant cut-out, Med. Eng. Phys. 35 (2013) 1442–1449.
[25] T.L. Mueller, S.E. Basler, R. Müller, G.H.v. Lenthe, Time-lapsed imaging of implant fixation failure in human femoral heads, Med. Eng. Phys. 35 (2013) 636–643.
[26] V.V. Kozey, S. Kumar, Compression behavior of materials: Part I. Glassy polymers, J. Mater. Res. 9 (2011) 2717–2726.
[27] D. Harding, F.Y. Tsai, R.Q. Gram, The properties of polyimide targets, LLE Review 92 (2002) 167–180.
[28] R. Mueller, S. Zhang, C. Zhang, R.P. Lively, S. Vasenkov, Relationship between long-range diffusion and diffusion in the ZIF-8 and polymer phases of mixed-matrix membrane by high field NMR diffusometry, J. Membr. Sci. 477 (2015) 123–130.
[29] R. Mueller, V. Hariharan, C. Zhang, R. Lively, S. Vasenkov, Relationship between mixed and pure gas self-diffusion for ethane and ethene in ZIF-8/6FDA-DAM mixed-matrix membrane by pulsed field gradient NMR, J. Membr. Sci. 499 (2016) 12–19.
[30] S. Friebe, A. Mundstock, K. Volgmann, J. Caro, On the better understanding of the surprisingly high performance of Metal−Organic framework-based mixed-matrix membranes using the example of uio-66 and Matrimid, ACS Appl. Mater. Interfaces 9 (2017) 41553–41558.
[31] L. Sheng, C. Wang, F. Yang, L. Xiang, X. Huang, J. Yu, L. Zhang, Y. Pan, Y. Li, Enhanced C_3H_6/C_3H_8 separation performance on MOF membranes through blocking defects and hindering framework flexibility by silicone rubber coating, Chem. Commun. 53 (2017) 7760–7763.
[32] A. Knebel, B. Geppert, K. Volgmann, D.I. Kolokolov, A.G. Stepanov, J. Twiefel, P. Heitjans, D. Volkmer, J. Caro, Defibrillation of soft porous metal-organic frameworks with electric fields, Science 358 (2017) 347–351.
[33] R.H. Vora, Process of Making a Shaped Article from Intermediate Molecular Weight Polyimides, CNA Holdings Inc, 1990.
[34] G.P. Robertson, M.D. Guiver, M. Yoshikawa, S. Brownstein, Structural determination of Torlon 4000T polyamide-imide by NMR spectroscopy, Polymer 45 (2004)

1111–1117.
[35] F. Zhou, W.J. Koros, Study of thermal annealing on Matrimid fiber performance in pervaporation of acetic acid and water mixtures, Polymer 47 (2006) 280–288.
[36] L. Xu, C. Zhang, M. Rungta, W. Qiu, J. Liu, W.J. Koros, Formation of defect-free 6FDA-DAM asymmetric hollow fiber membranes for gas separations, J. Membr. Sci. 459 (2014) 223–232.
[37] M. Dvoyashkin, J. Zang, G.I. Yucelen, A. Katihar, S. Nair, D.S. Sholl, C.R. Bowers, S. Vasenkov, Diffusion of tetrafluoromethane in single-walled aluminosilicate nanotubes: pulsed field gradient NMR and molecular dynamics simulations, J. Phys. Chem. C 116 (2012) 21350–21355.
[38] R.M. Cotts, M.J.R. Hoch, T. Sun, J.T. Markert, Pulsed field gradient stimulated echo methods for improved NMR diffusion measurements in heterogeneous systems, J. Magn. Reson. 83 (1989) 252–266.
[39] J. Kärger, D.M. Ruthven, D.N. Theodorou, Diffusion in Nanoporous Materials, Wiley-VCH Verlag GmbH & Co. KGaA, Weinheim, Germany, 2012.
[40] J. Kärger, H. Pfeifer, W. Heink, Principles and application of self-diffusion measurements by NMR, Adv. Magn. Reson. 12 (1988) 1–89.
[41] E.O. Stejskal, J.E. Tanner, Spin diffusion measurements: spin echoes in the presence of a time-dependent field gradient, J. Chem. Phys. 42 (1965) 288–292.
[42] P.T. Callaghan, D. MacGowan, K.J. Packer, F.O. Zelaya, Influence of field gradient strength in NMR studies of diffusion in porous media, Magn. Reson. Imaging 9 (1991) 663–671.
[43] J. Kärger, NMR self-diffusion studies in heterogeneous systems, Adv. Colloid Interface Sci. 23 (1985) 129–148.
[44] D. Wijesekera, T. Stait-Gardner, A. Gupta, J. Chen, G. Zheng, A.M. Torres, W.S. Price, A complete derivation of the kärger equations for analyzing NMR diffusion measurements of exchanging systems, Concepts Magn. Reson. (2019) 47A.
[45] E.M. Forman, B.R. Pimentel, K.J. Ziegler, R.P. Lively, S. Vasenkov, Microscopic diffusion of pure and mixed methane and carbon dioxide in ZIF-11 by high field diffusion NMR, Microporous Mesoporous Mater. 248 (2017) 158–163.
[46] O. Geier, R.Q. Snurr, F. Stallmach, J. Kärger, Boundary effects of molecular diffusion in nanoporous materials: a pulsed field gradient nuclear magnetic resonance study, J. Chem. Phys. 120 (2004) 367.
[47] P.P. Mitra, P.N. Sen, L.M. Schwartz, Short-time behavior of the diffusion coefficient as a geometrical probe of porous media, Phys. Rev. B Condens. Matter 47 (1993) 8565–8574.
[48] P.P. Mitra, P.N. Sen, Effects of microgeometry and surface relaxation on NMR pulsed-field-gradient experiments: simple pore geometries, Phys. Rev. B Condens. Matter 45 (1992) 143–156.
[49] M. Krutyeva, X. Yang, S. Vasenkov, J. Kärger, Exploring the surface permeability of nanoporous particles by pulsed field gradient NMR, J. Magn. Reson. 185 (2007) 300–307.
[50] A. Baniani, C. Chmelik, E.M. Forman, L. Fan, K.J. Ziegler, E. Zhou, F. Zhang, R. Lyndon, R.P. Lively, S. Vasenkov, Anomalous relationship between molecular size and diffusivity of ethane and ethylene inside crystals of zeolitic imidazolate framework-11, J. Phys. Chem. C 123 (27) (2019) 16813–16822, https://doi.org/10.1021/acs.jpcc.9b03933.